End Anchors for Continuously-Reinforced Concrete Pavements

R.A. MITCHELL, Highway Research Engineer, Virginia Council of Highway Investigation and Research (Now with National Bureau of Standards, Washington, D.C.)

Unrestrained end sections of continuously-reinforced concrete pavements have been observed to move several inches longitudinally due to thermal, shrinkage, or swelling strains. During the last few years a number of continuous slabs have been provided with subgrade anchors of various configurations to prevent these large end movements. This paper reports an experimental and theoretical study to develop guidelines for selecting and designing a suitable end anchor system.

A full-scale experimental investigation of two different end anchor configurations—a cylindrical pile-shaped anchor and a rectangular solid-shaped anchor—was conducted. Four test anchor units were subjected to a horizontal thrust applied by a jacking frame at the pavement slab level. Two of the test units were rigidly attached to a 15-ft length of 10-in. thick slab to simulate the interacting anchor-pavement system. The other two test anchor units were without attached slab. Loads, deflections, and rotations were measured.

A theoretical analysis has been developed for the elastic and plastic range of end anchor response. The more complex theoretical solutions have been presented in the form of curves for use in design.

•A CONTINUOUSLY-REINFORCED concrete pavement slab may expand or contract due to changes in temperature, moisture, chemical reaction, or mechanical stress. The resulting movement of the slab relative to its subgrade creates frictional stresses that oppose the movement. These subgrade frictional stresses prevent the development of a part of the potential slab strain but not all of it.

The movements discussed here are longitudinal expansions or contractions at the ends of a long slab. Movements of as much as 4 in. have been observed at the ends of continuously-reinforced concrete slabs (10). Such large movements must be either restrained or accommodated by expansion joints. Expansion joints capable of accommodating such movements are rather elaborate and may require considerable maintenance expenditure.

Zuk proposed that subgrade anchors be used to prevent excessive end movement and since that time a number of end anchor systems have been built in several States. Figure 1 shows a longitudinal section of the type of system that has commonly been used. The depths of vertical anchor units have ranged from 1 to 8 ft, and the thicknesses from 1 to 2 ft. Rectangular units extending the full width of the pavement slab and vertical cyclindrical units have been used (2).

There have been instances of conventional jointed concrete pavement expanding and exerting damaging forces against bridge structures. Such forces have been known to push abutments and piers out of alignment, to shear anchor bolts, and to move superstructures. To prevent these excessive expansions some States have used subgrade anchors. Texas, for example, has installed a large number of end anchor systems

Paper sponsored by Committee on Rigid Pavement Design.

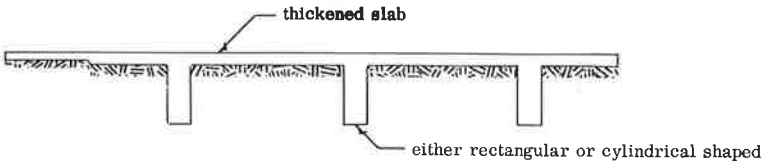

Figure 1. Longitudinal section of anchor system.

with jointed pavement as well as with continuously-reinforced pavement (4).

The study reported here was primarily concerned with subgrade anchor systems for use with continuously-reinforced concrete pavement, and the theoretical analyses and experimental investigation are discussed from that viewpoint. In a later section of the paper, subgrade anchors are discussed in relation to their possible use in jointed pavements.

The objective of the study was to develop a rational analysis of end anchor units and of systems of anchor units in series. A theoretical and an experimental investigation were conducted. In the theoretical phase the elements of the problem that are of most direct interest to the designer were considered. The experimental phase, which was considerably more limited in scope than the theoretical phase, included a full-scale field loading test of two different configurations of anchor unit.

LONGITUDINAL MOVEMENT OF PAVEMENT SLAB

Figure 2 shows some of the measurements of longitudinal movement along an experimental continuously-reinforced concrete pavement reported by Van Breemen (9). The horizontal scale represents the slab length of 5,130 ft. The vertical scale indicates the longitudinal movement of various points. Movement to the right is plotted above the abscissa. Thus, contraction of the left end is plotted above; and contraction of the right end is plotted below. The maximum movement is at each end, and the movement decreases at a decreasing rate to practically zero a few hundred feet from the end, as would be expected.

An explanation for the predominant nature of the curves in Figure 2 can be developed by examination of an idealized mechanical model. In Figure 3a the model represents one-half the length of a long slab having the following properties:

1. Uniform thickness, density, and linear elastic properties;
2. Uniform volume change due to temperature, moisture, etc., if not restrained by forces external to slab; and
3. Uniform friction coefficient relative to subgrade on which it is supported.

If there is no volume change due to temperature, moisture, etc., the only forces acting on the slab are its weight and the vertical subgrade reaction to that weight. If, however, there is longitudinal expansion or contraction of the slab, there is a uniform frictional stress throughout the region of longitudinal movements. The frictional stress acts on the slab in the direction opposite to the direction of movement.

Because the slab is assumed uniformly linear elastic, the components of horizontal strain due to different causes can be considered separately. Consider the case of the slab contracting due to temperature decrease T. The horizontal strain at any point due to temperature change is

$$\epsilon_t = -\alpha T \tag{1}$$

in which α = coefficient of thermal expansion.

If the orgin of the x-axis is at the free end of the slab, the strain due to uniform subgrade is

$$\epsilon_f = \frac{\mu w x}{AE} \tag{2}$$

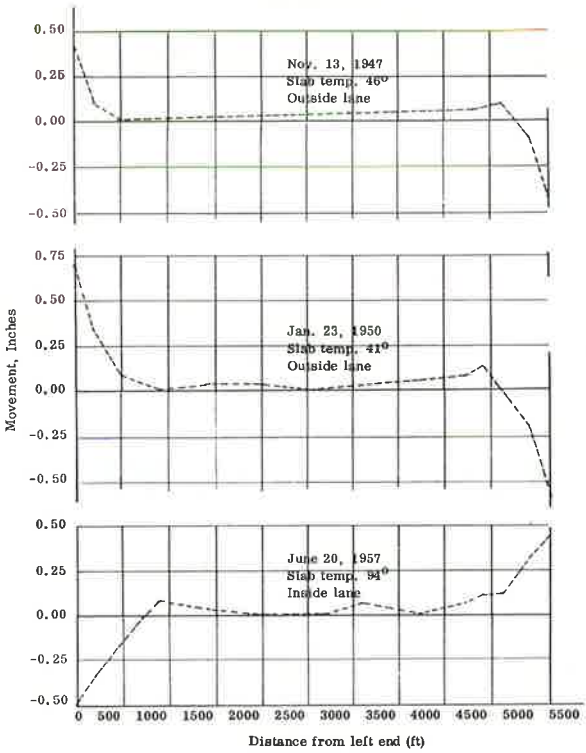

Figure 2. Movement of continuously-reinforced concrete pavement in New Jersey (9).

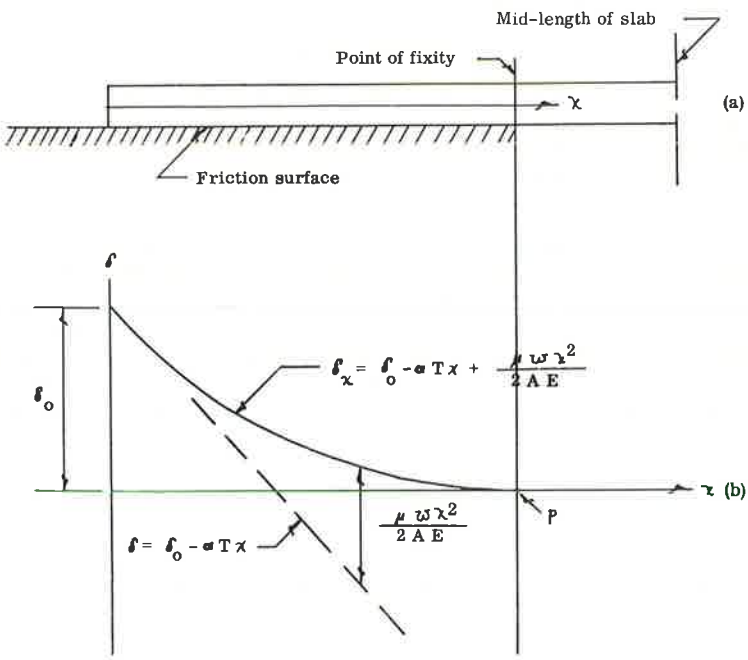

Figure 3. Idealized model of continuously-reinforced slab.

in which

μ = constant coefficient of friction;
w = slab weight per unit area;
A = slab cross-sectional area per unit width; and
E = elastic modulus.

The horizontal movement of a point on the slab relative to the end of the slab is therefore

$$\delta_{tf} = \delta_t + \delta_f = -\int_0^x \alpha T \, dx + \int_0^x \frac{\mu w x}{AE} \, dx$$

$$= -\alpha Tx + \frac{\mu w x^2}{2AE} \tag{3}$$

The total movement including the movement of the slab end δ_o is thus

$$\delta_x = \delta_o - \alpha Tx + \frac{\mu w x^2}{2AE} \tag{4}$$

This function is plotted in Figure 3b. At point x = p the curve is horizontal. Beyond that point there is no movement of the slab and no net strain. The strain due to temperature change is numerically equal (but of opposite sign) to that due to friction stress. In Figure 3b the three terms of Eq. 4 are separately indicated. The δ_x curve is tangent to the δ_t curve at x = 0, and is tangent to the x-axis at x = p. The conditions of zero strain and movement at x = p yield the two equations:

$$-\alpha T + \frac{\mu w}{AE} p = 0 \tag{5}$$

and

$$\delta_o - \alpha T p + \frac{\mu w}{2AE} p^2 = 0 \tag{6}$$

These simultaneous equations yield the solutions

$$p = \frac{AE}{\mu w} \alpha T \tag{7}$$

and

$$\delta_o = \frac{AE}{2 \mu w} (\alpha T)^2 \tag{8}$$

The amount of horizontal movement of the end of the slab could be further reduced by the addition of a horizontal force P at the slab end. The horizontal strain due to P would be P/AE and the movement of any point would be Px/AE.

This additional restraint would modify Eqs. 5 and 6 to

$$-\alpha T + \frac{P}{AE} + \frac{\mu w}{AE} p = 0 \tag{9}$$

$$\delta_o - \alpha T p + \frac{P}{AE} p + \frac{\mu w}{2AE} p^2 = 0 \tag{10}$$

The distance to the point of no movement would be

$$p = \frac{AE}{\mu w} \left(\alpha T - \frac{P}{AE} \right) \tag{11}$$

and the end movement would be

$$\delta_o = \frac{AE}{2\mu w}\left(\alpha T - \frac{P}{AE}\right)^2 \tag{12}$$

If the force P is applied at some distance h<p from the slab end the corresponding end movement would be

$$\delta_o = \frac{AE}{2\mu w}\left(\alpha T - \frac{P}{AE}\right)^2 + \frac{Ph}{AE} \tag{13}$$

If several horizontal forces were applied at various distances h_n < p from the slab end the resulting free end movement would be

$$\delta_o = \frac{AE}{2\mu w}\left(\epsilon - \sum_{n=1}^{K}\frac{Pn}{AE}\right)^2 + \sum_{n=1}^{K}\frac{Pn\,hn}{AE} \tag{14}$$

in which

ϵ = sum of strains due to temperature, moisture, etc. (i.e., αT in previous discussion);
P_n = various horizontal forces (P_1, P_2, ..., P_K); and
h_n = distances to corresponding horizontal forces (h_1, h_2, ..., h_K).

This equation for an idealized slab model is now examined in relation to the real problem of preventing excessive movement of a continuous pavement slab.

Experimental data (5) indicate that subgrade friction increases at a decreasing rate with an increasing movement of the slab (Fig. 4). Thus, Eq. 14, which was developed for a constant friction coefficient μ, would give only a rough approximation of actual end movement. In a later section of this paper an analysis is presented that takes into account this friction variation.

The last term of Eq. 14 indicates that the smaller the distance h to the point of application of a force P the more effective the force. This would be true whatever the nature of the force mechanism. If the force P is developed by passive resistance of a subgrade anchor, such an anchor would in general develop a greater force if located nearer the slab end where movement is greater. Of course, there is a limiting minimum spacing between anchor units beyond which the individual units interfere with adjacent ones. But, an anchor system is most efficient when the units are bunched at that minimum limiting spacing near the slab end. The determination of the minimum spacing is discussed later.

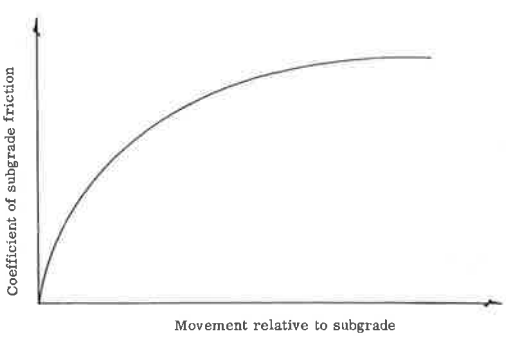

Figure 4. General nature of subgrade friction-movement relationship.

THEORY OF SUBGRADE ANCHOR RESISTANCE

The resistance of the slab to rotation of the slab anchor joint is considered first. Then the elastic and later the plastic resistance of the vertical anchor to horizontal deflection are examined. Plastic behavior is discussed particularly as it relates to minimum anchor spacing. Finally, the requirements for the bending and shear strengths of the reinforced concrete elements are considered.

The entire analysis is made for a longitudinal cross-section element of 1-in. width. A condition of plane strain is assumed to exist.

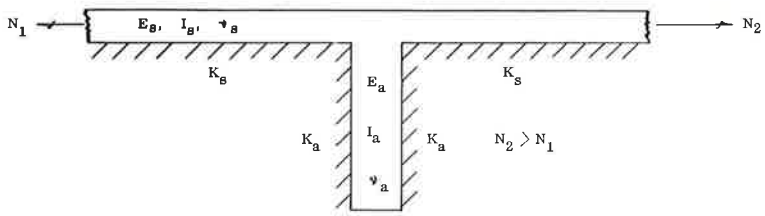

Figure 5. Assumed elastic system.

Elastic Analysis

Figure 5 shows the assumed elastic system. The symbols ν, E, I and K represent Poisson's ratio, the elastic modulus of the concrete, the moment of inertia of the concrete member, and the modulus of reaction of the subgrade soil, respectively. The subscripts s and a identify the properties of the slab and anchor, respectively. The soil modulus K is assumed to be defined by

$$p = b K_o y = Ky \tag{15}$$

in which

- p = normal pressure at soil-concrete interface due to deflection;
- y = transverse deflection of slab or anchor;
- b = width of the deflected concrete elements (1 in. for this analysis);
- K_o = soil modulus, constant ratio of pressure to deflection for any width of elements; and
- K = abbreviation for bK_o in this analysis (lb per cu in.).

It is assumed that the weight and stiffness of the system are sufficient to prevent significant vertical movement of the joint. Because $N_2 > N_1$ the slab is displaced to the right. As the top of the anchor is deflected horizontally, rotation of the anchor is partially restrained by the slab and a bending is induced at the joint. Hetenyi (3) gives a solution for the deflection of an infinitely long beam with axial load N and transverse moment M_o (Fig. 6) as

$$y = \frac{M_o}{4EI} \frac{e^{-\alpha x}}{\alpha\beta} \sin \beta x \tag{16}$$

in which

$$\alpha = \sqrt{\sqrt{\frac{K}{4EI}} + \frac{N}{4EI}}$$

$$\beta = \sqrt{\sqrt{\frac{K}{4EI}} - \frac{N}{4EI}}$$

The corresponding rotation at $x = 0$ is

$$\theta_o = \frac{M_o}{4EI\alpha} \tag{17}$$

The ratio of applied moment to rotation is

$$C = \frac{M_o}{\theta_o} = 4EI\alpha$$

$$= 4EI\sqrt{\sqrt{\frac{K}{4EI}} + \frac{N}{4EI}} \tag{18}$$

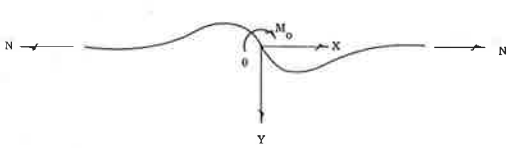

Figure 6. Infinite beam on elastic foundation with transverse applied moment.

To apply this solution to the present problem of plane strain, the effective stiffness of the slab must be modified to give

$$C = \frac{M_o}{\theta_o} = \frac{4 E_S I_S}{(1-\nu^2)} \sqrt{\sqrt{\frac{K_S (1-\nu^2)}{4 E_S I_S}} + \frac{N (1-\nu^2)}{4 E_S I_S}} \qquad (19)$$

In an effort to simplify this relationship for the present problem, the importance of N in relation to C was studied. It was found that for a wide range of N (from a tension of 60,000 psi in 0.6 percent steel to a compression of 5,000 psi in concrete) and for a wide range of other properties (that is, $\nu = 0.15$; $EI = 15 \times 10^7$ to 45×10^7 lb-in.^{2}; K = 100 to 1,000 psi) the maximum variation in C is about 10 percent. This was considered sufficient justification for dropping N in Eq. 19 to obtain

$$C = \frac{M_o}{\theta_o} = \sqrt[4]{\left[\frac{E_S t_S^3}{3 (1-\nu^2)}\right]^3} \cdot K_S \qquad (20)$$

in which t_S = slab thickness.

Figure 7 is a plot of C vs t_S for $E_S = 4 \times 10^6$ psi and $\nu = 0.15$.

There is also a question of C being reduced due to interference from an adjacent anchor unit. The slope at any point along the infinitely long beam shown in Figure 6 is (3, p. 129).

$$\theta_x = \frac{M_o}{4 EI} \frac{1}{\alpha \beta} e^{-\alpha x} (\beta \cos \beta x - \alpha \sin \beta x) \qquad (21)$$

The point at which $\theta_x = 0$, x_c, may be found by setting the right side of Eq. 21 equal to zero. This gives

$$x_c = \frac{1}{\beta} \arctan \frac{\beta}{\alpha} \qquad (22)$$

The change in N throughout the vicinity of x = 0 is assumed to be sufficiently small to permit superposition of elastic solutions. Thus, the rotation curves due to two adjacent transverse moments can be added directly to get the rotation due to the pair. By doing this, it can be readily demonstrated that, if two adjacent anchors are no closer than x_c, the rotation of one does not increase the rotation of the other and thus decrease the C-value of the other. To determine a reasonable maximum value that x_c might attain, Eq. 22 was used to determine x_c to be 52 in. for the rather extreme values: $N = 3 \times 10^3$ lb; $E_S I_S = 45 \times 10^7$ lb-in.^{2}; K = 100 psi; $\nu = 0.3$. The likelihood of anchors being placed closer than 52 in. seems rather remote.

Two solutions reported by Hetenyi (3) have been combined to give a solution for the anchor element (Fig. 8c). The equations for deflection and rotation at the point x = 0 of the anchor element loaded with the horizontal force P (Fig. 8a) are

$$y_a = \frac{2 P \beta}{K} \left(\frac{\sinh \beta H \cosh \beta H - \sin \beta H \cos \beta H}{\sinh^2 \beta H - \sin^2 \beta H}\right) = \frac{2 P \beta}{K} g_1 \qquad (23)$$

and

$$\theta_a = -\frac{2 P \beta^2}{K} \left(\frac{\sinh^2 \beta H + \sin^2 \beta H}{\sinh^2 \beta H - \sin^2 \beta H}\right) = \frac{2 P \beta^2}{K} g_2 \qquad (24)$$

in which

$$\beta = \sqrt[4]{\frac{K (1-\nu^2)}{4 EI}}$$

H = anchor depth.

The corresponding equations for the anchor element loaded with the moment Mo (Fig. 8b) are

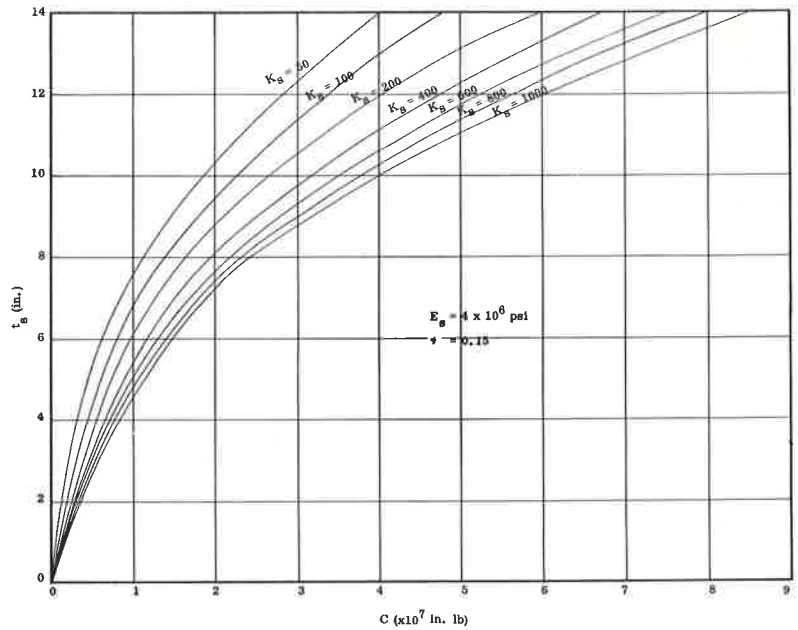

Figure 7. Moment-rotation ratio vs slab thickness.

$$y_b = -\frac{2 M_o \beta^2}{K}\left(\frac{\sinh^2 \beta H + \sin^2 \beta H}{\sinh^2 \beta H - \sin^2 \beta H}\right) = -\frac{2 M_o \beta^2}{K} g_2 \qquad (25)$$

and

$$\theta_b = \frac{4 M_o \beta^3}{K}\left(\frac{\sinh \beta H \cosh \beta H + \sin \beta H \cos \beta H}{\sinh^2 \beta H - \sin^2 \beta H}\right) = \frac{4 M_o \beta^3}{K} g_3 \qquad (26)$$

Eqs. 23 through 26 can be combined to give the deflection and rotation at x = 0 for the combined loading condition (Fig. 8c).

$$y_c = \frac{2 P \beta}{K} g_1 - \frac{2 M_o \beta^2}{K} g_2 \qquad (27)$$

$$\theta_c = \frac{4 M_o \beta^3}{K} g_3 - \frac{2 P \beta^2}{K} g_2 \qquad (28)$$

The moment and rotation at the top of the anchor are numerically equal to the moment and rotation of the slab at the joint. But the moment acting on the anchor is in the direction opposite joint rotation, whereas the moment acting on the slab is in the direction of rotation. Thus, from Eq. 20,

$$\theta_c = \frac{4 M_o \beta^3}{K} g_3 - \frac{2 P \beta^2}{K} g_2 \frac{M_o}{C}$$

or

$$M_o \left[\frac{4 \beta^3}{K} g_3 + \frac{1}{C}\right] - \frac{2 P \beta^2}{K} g_2 = 0 \qquad (29)$$

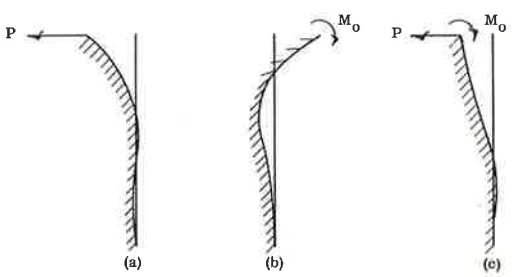

Figure 8. Elastic model of vertical anchor.

Eq. 27 can be subtracted from Eq. 29 to eliminate M_o, thus giving y_c in terms of P, β, H, K, and C as

$$y_c = \frac{2P\beta}{K_a} \left[g_1 - \frac{2\beta^3 g_2^2}{(4\beta^3 g_3 + \frac{K}{C})} \right] \tag{30}$$

This equation can be rearranged and divided by H to get

$$\frac{P}{K_a y H} = \frac{1}{2\beta_a H \left[g_1 - \frac{2\beta_a^3 g_2^2}{(4\beta_a^3 g_3 + \frac{K_a}{C})} \right]} \tag{31}$$

The subscripts a that were neglected for the derivation of Eq. 31 are inserted in the equation to avoid confusion. The functions g_1, g_2, and g_3 are functions of β_a H only. The factor y in Eq. 31 is equal to the horizontal movement of the slab at the joint, δ, and the force P is equal to the anchor force. Plots of $P/K_a H \delta$ vs H for different values of β_a and K_a/C are given in Figures 9 a-d.

An infinitely stiff anchor of any length, rigidly fixed at the pavement joint, would have the properties,

$$\beta = 0, \quad C = \infty, \quad \text{and} \quad \frac{P}{K_a H \delta} = 1$$

The curves in Figure 9 show how this quantity is decreased by a decrease in C or an increase in β_a or H. For design analysis the curves can be used to determine the anchor force P for an elastic system after the quantities δ, H, K_a, β_a, and C have been determined. A plot of β_a vs anchor thickness t_a for $E_a = 4 \times 10^6$ and $\nu = 0.15$ is given in Figure 10.

Plastic Analysis

The discussion of slab longitudinal movement showed that anchor units should be closely bunched near the slab free end. One objective of the following analysis is to determine the limiting minimum spacing beyond which closer spacing would result in no greater efficiency of the anchor system. The other objective is to determine the limiting plastic yield strength of anchor units placed at that theoretical optimum spacing. For this problem it is assumed that the anchor units are far enough apart that elastic displacement within the soil mass at one unit, due to forces exerted by other units, is insignificant.

The two adjacent anchor units shown in Figure 11a may be used as an example. If there is no horizontal movement of the anchor units, the planes ab, cd, and ef are acted on by the "at rest" earth pressure, and the shear stress along plane bd is zero. As the anchors are moved to the left the net force on plane ab is decreased, the net force on cd is increased, and shear stress is induced along at least parts of planes bd and ac. It is assumed that if movement is continued there will eventually be plastic shear flow, characterized by no increase in shear stress, along one or more of the three planes bg, bd, and dh. The precise locations and curved shapes of planes bg and dh are not specified. The assumed flow directions are shown in Figure 11a by arrows.

Figure 11b shows the net horizontal forces acting on the soil body abdc. Equilibrium conditions require that

$$S - F_t = P_p - P_a \tag{32}$$

This equation necessarily holds throughout the elastic and plastic range of response. For the limiting plastic values of P_a and P_p, designated P_a' and P_p', to develop, it is necessary that the value of $S - F_t$ be sufficiently large to hold the body abdc in equilibrium. That is, if the anchors are too close together, shear flow will develop along plane bd before it does along planes bg and dh.

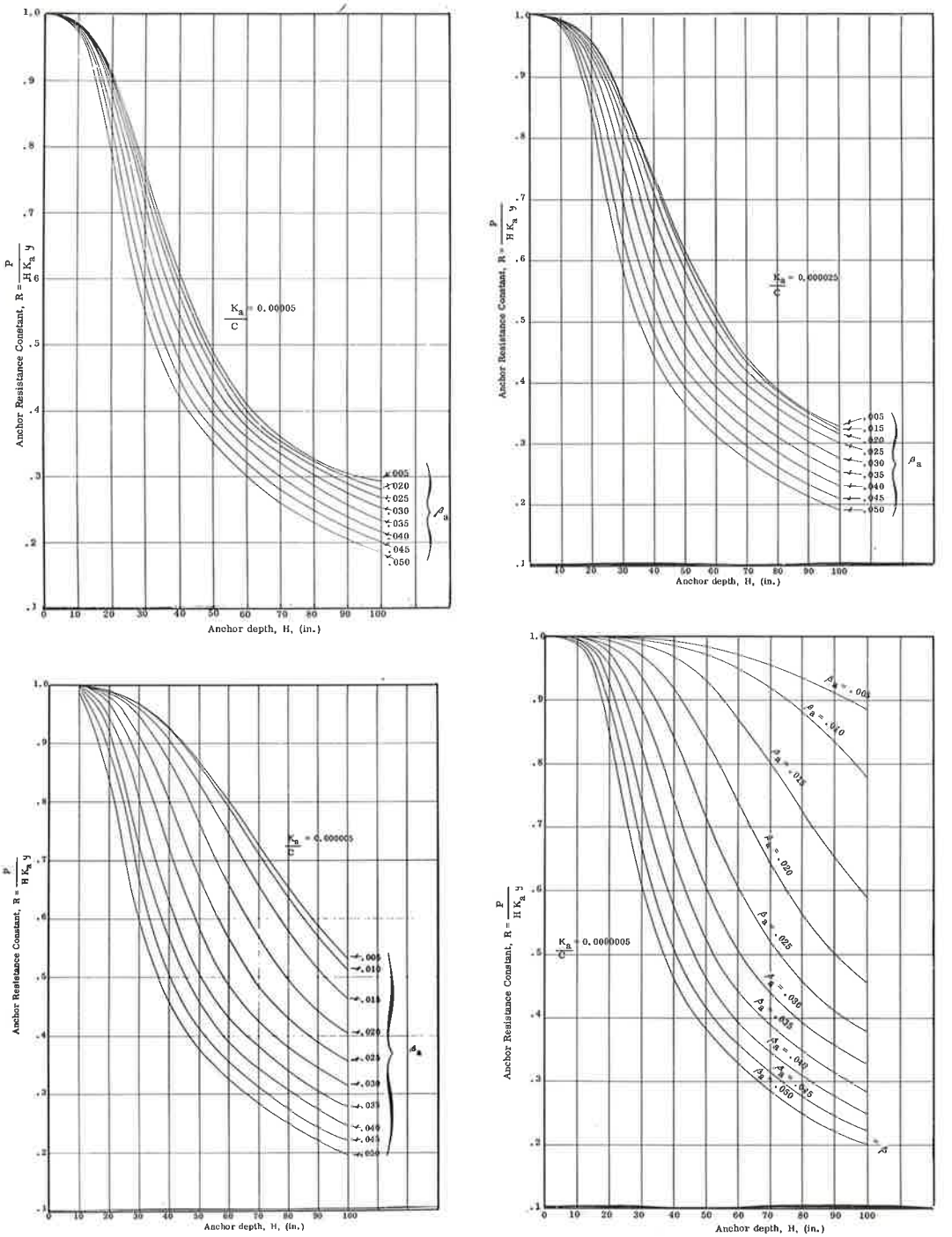

Figure 9. Resistance constant vs anchor depth.

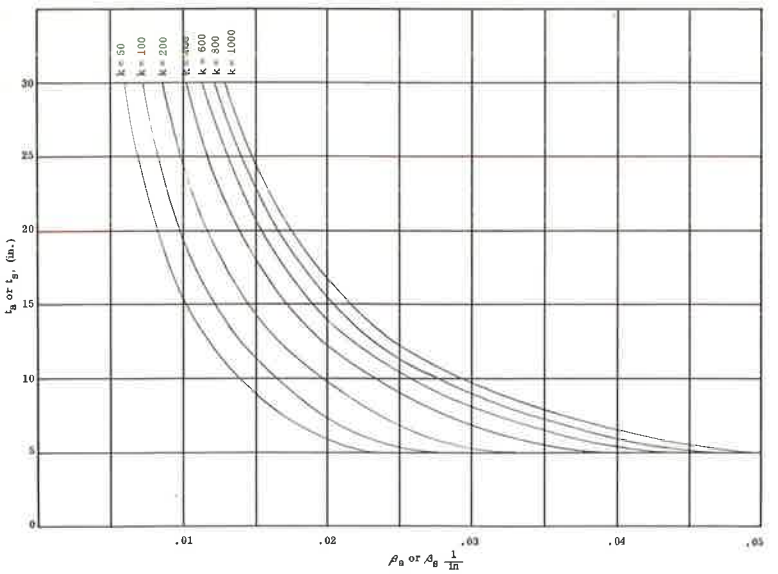

Figure 10. Characteristic β vs element thickness (slab or anchor).

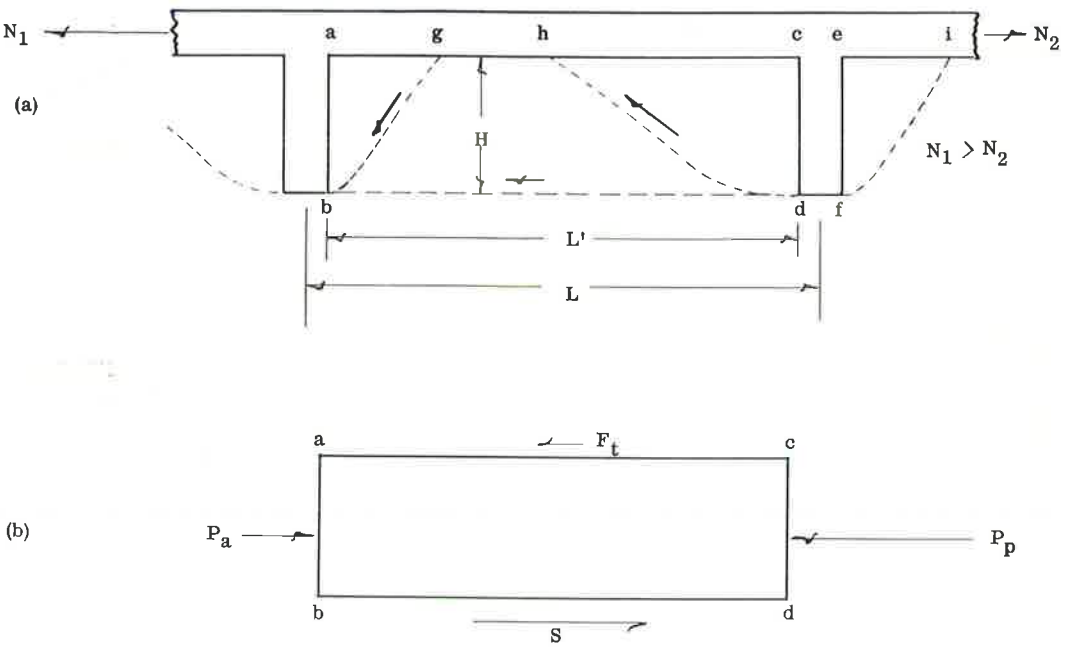

Figure 11. Plastic model of adjacent anchors.

If the subgrade soil properties are uniform and if there is plastic flow along planes bg, dh, and fi, equal forces P_a' are acting on planes ab and ef, and the net horizontal force on anchor cdfe is $P_p' - P_a'$. That is the limiting maximum force that can be developed by an anchor. If the anchor units are so far apart that plastic shear flow does

not develop along plane bd when the limiting anchor force $P_p' - P_a'$ is developed, the anchor system does not develop the full potential strength of the subgrade soil. This argument leads to the conclusion that, if movement is sufficient to develop plastic flow along either of planes bg, bd, dh, or fi, the optimum anchor spacing is that spacing at which shear flow will develop on all four planes. At that spacing the following equation will apply:

$$S' - F_t = P_p' - P_a' \tag{33}$$

in which S' = limiting plastic shear force along bd.

The force F_t acting along plane ac is assumed to be equal to the product of the slab weight and some uniform soil property constant G. The limiting shear force S' acting along plane bd is assumed to consist of a component equal to the product of the soil constant G and the weight of material above plane bd and a component that is independent of the weight of the material above bd. Thus S' may be thought of as consisting of a component F_t and a component that is independent of the slab weight, say P_h'; that is,

$$S' = P_h' + F_t \tag{34}$$

Substitution of Eq. 34 into Eq. 33 gives

$$P_h' = P_p' - P_a' \tag{35}$$

in which P_h' = component of limiting shear stress along plane bd that is independent of slab weight.

It is fully realized that the movement of a real two anchor system such as shown in Figure 11 would very likely not be characterized by shear flow initially developing along planes bg, bd, dh, and fi at the same time. Also, the rates of increase of the forces P_h, P_p, and P_a from zero to their limiting values P_h', P_p' and P_a' would in general not remain in constant ratio. Therefore, the theoretical optimum spacing of anchor units for movements large enough to induce plastic flow would not necessarily be the optimum spacing for lesser movements. And the movements of all or at least some of the units of a pavement anchor system would likely remain less than that required for plastic flow. But if the ratios of the rates of increase of P_h, P_p, and P_a are not too variable throughout their entire range, then the optimum anchor spacing throughout the range would not be too different.

The reasoning leading to Eq. 35 would seem to be valid regardless of the precise nature of the boundary conditions along the surface bacd. But to simplify the problem for a numerical parameter analysis, the following rather extreme assumptions are made.

It is assumed that the conditions at the boundary of the soil body, abdc (Fig. 12) due

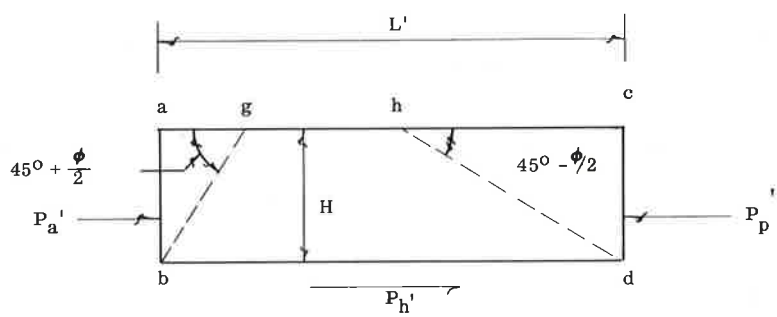

Figure 12. Soil in assumed Rankine state of plastic equilibrium between anchors.

to the weight and stiffness of the pavement slab and anchor units, are compatible with the Rankine theory of earth pressure (6, pp. 26-48). This assumption includes the conditions that there be no shear stress along planes ab and cd and that there be no stress along plane ac.

In Rankine's theory it is assumed that the limiting shear stress on surfaces of plastic shear flow is given by Coulomb's empirical equation

$$\gamma = c + \bar{\sigma} \tan \phi \tag{36}$$

in which

c = shearing resistance that is independent of effective normal stress;
$\bar{\sigma}$ = effective normal stress transferred by intergranular contact along shear plane; and
ϕ = angle of internal friction.

The theory assumes that c and ϕ are material properties that are constant for any direction of shear, for any magnitude of effective normal stress $\bar{\sigma}$, and at any point in the shear zone. This assumption is only approximately correct even if c and ϕ are selected on the basis of careful test (1, 6). But if c and ϕ are determined by tests closely approximating the stress, stress history, and moisture conditions of the anchor system subgrade, the results should be sufficiently accurate for engineering design purposes.

Figure 12 shows the soil body abdc in the assumed Rankine state of plastic equilibrium and for which Eq. 35 will be assumed to apply. There is shear flow along planes bg, dh, and bd. According to the Rankine theory (6, pp. 26-48) the inclined planes are at angles of $45^0 \pm \phi/2$ and the active and passive earth forces are

$$P_a' = \frac{\gamma_S H^2}{2 \tan^2 (45^0 + \phi/2)} - \frac{2 c H}{\tan (45^0 + \phi/2)} \tag{37}$$

$$P_p' = \frac{\gamma_S H^2}{2} \tan^2 (45^0 + \phi/2) + 2 c H \tan (45^0 + \phi/2) \tag{38}$$

Eq. 37 as written assumes that the soil can exert a normal tensile stress along the upper part of plane ab down to a depth equal $2 c/\gamma_S \tan (45^0 \text{ M } \phi/2)$. Because soil in general does not develop significant direct tensile strength it is commonly assumed that any direct tensile stress included in Eq. 37 is zero. This is accomplished by the addition of the term $2 c^2/\gamma$ to Eq. 37 (8 p. 149) to get

$$P_a' = \frac{\gamma_S H^2}{2 \tan^2 (45^0 + \phi/2)} - \frac{2 c H}{\tan (45^0 + \phi/2)} + \frac{2 c^2}{\gamma} \tag{39}$$

If the depth H is less than the quantity $2 c/\gamma_S \tan (45^0 + \phi/2)$ it is commonly assumed that the active force $P_a' = 0$.

When plane bd (Fig. 12) is in a state of plastic flow it is assumed that the shear stress is given by Eq. 36. The total shear force on plane bd is thus

$$P_S' = L' (c + \bar{\sigma} \tan \phi) \tag{40}$$

For this application it can be safely assumed that strain rate is slow enough that water pressure in the zone of shear yielding is unaffected by the shear strain. The effective normal stress $\bar{\sigma}$ is given by

$$\bar{\sigma} = \sigma - h_w \gamma_w \tag{41}$$

in which

σ = total normal stress on plane bd;

γ_w = unit weight of water; and
h_w = height of soil saturation above plane bd.

If the soil is uniformly saturated up to the subgrade surface the effective normal stress on plane bd is

$$\bar{\sigma} = H\ \gamma - H\ \gamma_w = H\ (\gamma - \gamma_w) \tag{42}$$

in which γ = unit weight of saturated soil. If the soil is unsaturated throughout the depth H the effective normal stress on bd is $\bar{\sigma} = H\ \gamma$. If $\bar{\gamma}$ designates the effective unit weight of the soil, that is $(\gamma - \gamma_w)$ for saturated soil and γ for unsaturated soil, the effective normal stress on plane bd for uniform soil conditions throughout the depth H is

$$\bar{\sigma} = \bar{\gamma}\ H \tag{43}$$

The corresponding shear force developed along bd is

$$P_s' = L'\ c + L'\ \bar{\gamma}\ H \tan \phi \tag{44}$$

By substituting Eqs. 38, 39, and 44 into Eq. 35 the optimum clear spacing between anchors L' can be determined to be

$$L' = \left\{ \frac{\frac{\bar{\gamma}\ H}{2\ c}\left[\tan^2\left(45^0 + \frac{\phi}{2}\right) - \tan^2\left(45^0 - \frac{\phi}{2}\right)\right] + 2\left[\tan\left(45^0 + \frac{\phi}{2}\right) + \tan\left(45^0 - \frac{\phi}{2}\right)\right] - \frac{2\ c}{H\bar{\gamma}}}{\frac{\gamma \tan \phi}{c} + \frac{1}{H}} \right\} \tag{45}$$

for the condition $H > \frac{2\ c}{\bar{\gamma}} \tan^2 (45^0 + \frac{\phi}{2})$.

The corresponding solution for the condition $H \leqq \frac{2\ c}{\bar{\gamma}} \tan (45^0 + \frac{\phi}{2})$ is

$$L' = \frac{\frac{\bar{\gamma}\ H}{2\ c} \tan^2\left(45^0 + \frac{\phi}{2}\right) + 2 \tan\left(45^0 + \frac{\phi}{2}\right)}{\frac{\bar{\gamma} \tan \phi}{c} + \frac{1}{H}} \tag{46}$$

Solutions to Eqs. 45 and 46 are shown in Figure 13 giving the ratio of L' to H for a wide range of values $\bar{\gamma}$, c, ϕ, and for anchor depths of 20 and 100 in. The curves for c = 0 and c = ∞ are the same for any values of H and $\bar{\gamma}$. It appears that all practical problems having H less than 100 would yield solutions within or very near the band of solutions shown in Figure 13b. Thus, according to this theory the anchors should be at least 2H apart. They could be spaced up to the vicinity of 5H for very strong soil without loss of efficiency. It is obvious that the curves in Figure 13 do not permit accurate linear interpolation, so Eq. 45 or 46 should be used for specific solutions that are not given by the curves.

If there is plastic shear flow along plane bd, the net force developed against an anchor unit such as cdfe in Figure 11a is Eq. 40. But a weakness of this analysis is that it does not predict the movement necessary to develop the full plastic resistance given by the equation. In an earlier section of this paper the elastic response of an anchor unit was analyzed. Here, the limiting case of plastic response was considered. But between the approximately linearly elastic range and the plastic flow range there is a range of behavior about which relatively little is precisely understood.

Figure 14 shows a load vs displacement curve of the type commonly assumed to exist for engineering analysis of subgrade structures. It is commonly assumed (for example, 7, p. 322) that the load-displacement curve follows a straight line such as 0_a up to a limiting elastic load P_e equal to one-half the limiting plastic load P_u. Beyond

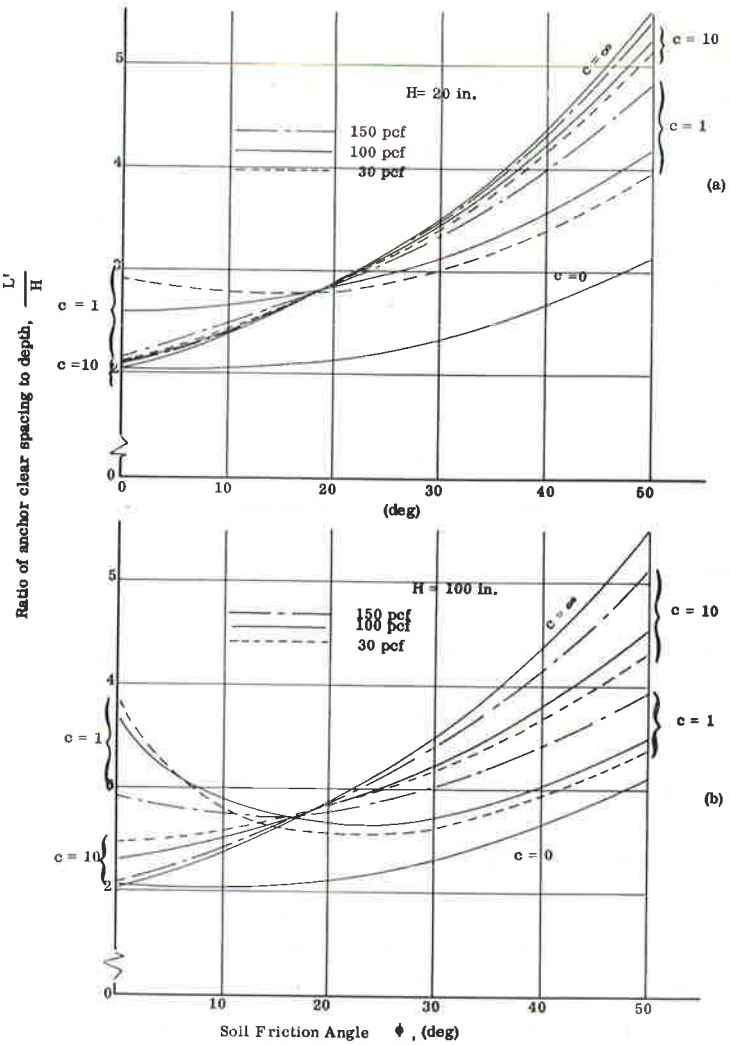

Figure 13. Theoretical optimum spacing-depth ratio for various anchor depths and soil properties.

that point, in accordance with experience, it is assumed that the curve bends appreciably to the extent that the minimum plastic displacement δ_u is several times the maximum elastic displacement δ_e. In the analysis of a pavement anchor system it is required that the anchor resistance P corresponding to a predetermined displacement δ be determined. Unless something is known of the shape of the curve bc (Fig. 14) or of the ratio of δ_u to δ_e it is proposed that the assumed anchor resistance be limited to one-half the plastic resistance. In the design procedure proposed in the next section of this paper the anchor force corresponding to a given deflection is determined by elastic analysis with the limitation that, if the force so determined exceeds one-half the limiting plastic force, the anchor resistance is taken to be one-half the plastic force.

Shear and Moment Analysis

To determine the shear and moment strength required in the anchor, the conditions

shown in Figure 15 are assumed. The force P is equal in magnitude to the anchor resistance force determined by elastic or plastic analysis as previously discussed. P is also the resultant of the subgrade horizontal pressure that is assumed to increase linearly with depth. The resulting moment at the top of the anchor, and applied to the slab, is

$$M_o = \frac{2}{3} PH \qquad (47)$$

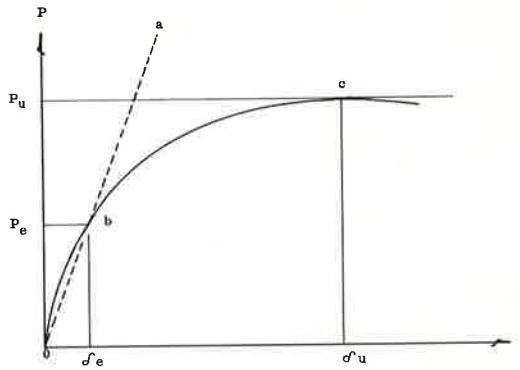

Figure 14. Load-displacement curve of type commonly assumed for engineering analysis.

The assumption of P acting at 2H/3 is rather arbitrary. P could actually act at a higher or lower point depending on anchor stiffness and soil deformation conditions. In the extreme limiting case P could act at the anchor bottom, but the assumption of P acting at 2H/3 is probably sufficiently conservative for engineering purposes.

The problem of shear and moment in the slab adjacent to the joint is more complex. It is complicated by such facts as (a) soil does not develop significant tensile strength, (b) axial loads and transverse traffic loads are acting along with anchor loads, and (c) bending and shear cracks might well develop near the joint. The complexity of the problem would seem to justify a trial and error approach; that is, design should be adjusted on the basis of careful observation of the performance of anchor joints in the field. The following analysis, based heavily on intuition and simplifying assumptions, is proposed for design guidance, subject to modification as indicated by field observations.

It is assumed that axial loads in the slab and traffic loads have negligible effect on the distribution of the shear and moment that is induced in the slab by the anchor moment. Hetenyi (3 p. 14) gives expressions for the deflection, rotation, moment, and shear of an infinitely long beam loaded with a concentrated transverse moment. His expressions, modified for plane strain conditions and with notation modified to conform with that used elsewhere in this paper, are

$$y = \frac{M_o \beta_s^2}{K_s} e^{-\beta_s x} \sin \beta x \qquad (48)$$

$$\theta = \frac{M_o \beta_s^3}{K_s} e^{-\beta_s x} (\cos \beta_s x - \sin \beta_s x) \qquad (49)$$

$$M = \frac{M_o}{2} e^{-\beta_s x} \cos \beta_s x \qquad (50)$$

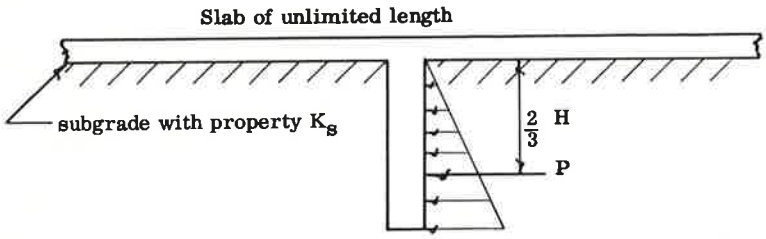

Figure 15. Assumed condition for moment and shear analysis.

$$V = \frac{-M_o}{2} \beta_S e^{-\beta_S x} (\cos \beta_S x + \sin \beta_S x) \quad (51)$$

in which

$$\beta_S = \sqrt[4]{\frac{K_S (1 - \nu^2)}{4 E_S I_S}}$$

x = distance from joint along slab.

A plot of β_S vs slab thickness t_S for $E_S = 4 \times 10^6$ psi and $\nu = 0.15$ is shown in Figure 10. Figure 16 shows the general shape of the curves corresponding to Eqs. 48 through 51. It is proposed that these four equations, with the modifications suggested in the following paragraph, be assumed to apply to the slab in the vicinity of an anchor.

Because the subgrade soil cannot actually develop tensile stress, it appears likely that the greater part of the shear and moment induced by the anchor will be balanced by the downward deflected side of the slab (Fig. 16). Therefore, it is recommended that the slab be designed to withstand double the moment and shear given by Eqs. 50 and 51. But if two adjacent anchors are closer together than two times the distance to the point of zero moment given by Eq. 50 (Fig. 16) the moment should be assumed zero midway between the anchors. It is recommended that reinforcing steel required for anchor-induced moment and shear be provided in addition to the normal continuous pavement reinforcing steel. It is also recommended that the slab thickness be sufficient to resist either the anchor-induced loads or the traffic loads, whichever is greater.

RECOMMENDED PROCEDURE FOR ANALYSIS AND DESIGN

The following paragraphs outline a recommended procedure for the analysis and design of an anchor system. At the end of this section a numerical example is presented. The reader may wish to refer to earlier sections for definitions of terms or for theoretical justification of some of the following.

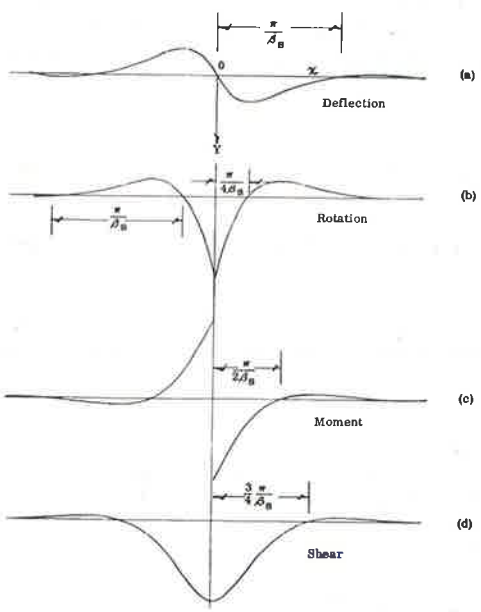

Figure 16. Response of infinite beam on elastic foundation due to transverse moment applied at x = 0.

Temperature, Moisture, or Chemical Strain. —An anchor system should be designed to accommodate a selected unit strain ϵ. This strain might be induced by changes in temperature, moisture, or chemical state of the pavement slab. A detailed study of these phenomena is beyond the scope of this paper, but considerable information on this subject is contained in the technical literature.

End Movement. —End movement δ_o should be assumed equal to the range of the expansion joint to be provided at the slab end. The greater the end movement, the smaller the required anchor forces. Thus, an expansion joint of the greatest range practical should be used.

Soil Properties. —The following properties of the subgrade soil in place must be determined or assumed:

1. Coefficient of vertical subgrade reaction under the slab, K_S.
2. Coefficient of horizontal subgrade reaction throughout the anchor depth K_a.
3. Angle of internal friction, ϕ.
4. Effective cohesion, c.

5. Effective unit weight of soil throughout the anchor depth, $\overline{\gamma}$, as defined for Eq. 43.

Subgrade Friction. —A curve of subgrade friction coefficient vs movement must be assumed.

Concrete Properties. —Poisson's ratio γ and the elastic modulus E must be determined or assumed.

Anchor Dimensions. —The selection of anchor dimensions would seem to require consideration of construction methods. Holes for cylindrical anchors can be dug with a power-driven auger. Rectangular trenches can be dug with a variety of trenching machines. Either shape can also be dug with hand tools. Of course the deeper an anchor is, the more resistance it can develop. Once the maximum bending moment and shear have been determined, the anchor dimensions should be checked for sufficiency.

Anchor Spacing. —It is recommended that the required clear spacing between anchor units be calculated using Eq. 45 or 46 or by reading directly from Figure 13. It is also recommended that the first anchor unit be located at a distance from the free end equal to the anchor depth. The latter recommendation is based more on intuition than on theoretical analysis.

Limiting Anchor Resistance. —The theoretical limiting anchor resistance P_s' can be calculated by Eq. 40. It is recommended that one-half that value be used as the maximum resisting force developed by a single anchor.

Anchor Bending Moment and Shear. —The maximum bending moment and shear in the anchor at the joint should be determined as discussed above under "Shear and Moment Analysis." The maximum shear is equal to the anchor force P. The maximum bending moment is assumed to be given by Eq. 47. At this point, the anchor dimensions should be checked for sufficiency.

Slab Thickness. —It is recommended that the slab be thick enough and reinforced enough to withstand double the moment and shear given by Eqs. 50 and 51. Steel re-

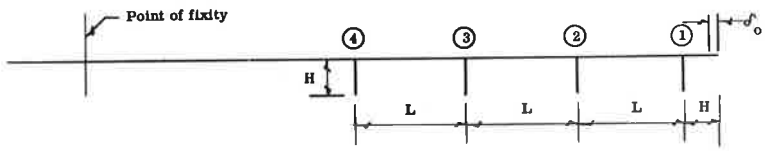

Figure 17. Line diagram of anchor system.

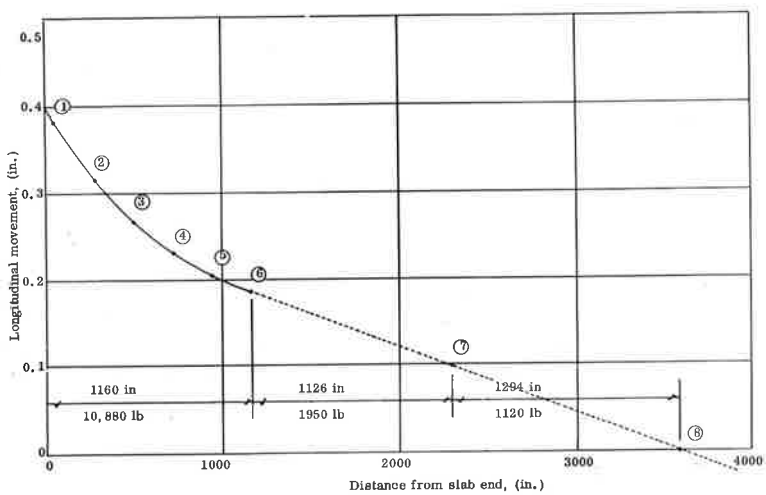

Figure 18. Longitudinal movement of slab in numerical example.

quired for anchor-induced moment and shear should be provided in addition to the regular continuous pavement reinforcing steel (the discussion under "Shear and Moment Analysis" gives further guidance on steel placement). Reinforcing steel should be checked for bond, minimum spacing, and cover before proceeding.

Joint Moment-Rotation Ratio. —A satisfactory approximation to the moment-rotation ratio C can be calculated using Eq. 20. If the concrete properties are in approximate agreement, the value of C can be read from Figure 7.

Elastic Anchor Resistance. —The value of the anchor characteristic β_a can be calculated using the definition given with Eq. 24 or it can be read from Figure 10 if the concrete properties are in approximate agreement. With βa, K_a, C, and H known, the value of the anchor resistance constant $R = P/H K_a \delta$ can be interpolated using Figure 9. The numerical example presented later illustrates interpolation among all four of the families of curves of Figure 9 to evaluate the anchor resistance constant R.

Longitudinal Movement Analysis. —After the preceding quantities have been determined the following steps can be performed to complete the anchor system analysis.

1. Determine movement δ_1 at point 1 (Fig. 17) as the end movement minus the movement at point 1 relative to the end; that is,

$$\delta_1 = \delta_0 - \epsilon H \tag{52}$$

2. Knowing R, H, K_a, and δ_1, compute the elastic resistance of anchor 1 using

$$P = R H K_a \delta_1. \tag{53}$$

The value of P must be compared to $P_S'/2$. The smaller of the two values should be used as the anchor resistance force P_1.

3. Determine movement δ_2 at point 2 (Fig. 17) as the movement δ_1 minus the movement at point 2 relative to point 1; that is,

$$\delta_2 = \delta_1 - \epsilon L + \frac{P_1 L}{AE} \tag{54}$$

4. Repeat step 2 to determine P_2.
5. Determine δ_3 to be

$$\delta_3 = \delta_2 - \epsilon L + (P_1 + P_2) \frac{L}{AE} \tag{55}$$

6. Repeat for additional anchors as necessary.
7. Plot a graph of δ vs position along slab, as in Figure 18. For a satisfactory design, the curve must become horizontal at some point at or above the horizontal axis, $\delta = 0$. If the curve becomes horizontal far above the horizontal axis, the system is overdesigned. The total axial force ΣP acting on the slab at some point beyond the last anchor unit must be equal to or greater than given by

$$\Sigma P = AE \epsilon \tag{56}$$

in which A is the cross-sectional area of that part of the slab beyond the last anchor. (A in Eq. 56 is not necessarily the same magnitude as A in Eq. 55.) That is, the total restraining force must be sufficient to develop a mechanical strain equal to the temperature, moisture, or chemical strain. The total force consists of anchor forces and the subgrade friction forces acting in the zone between the last anchor and the point of fixity. For numerical analysis, the distributed subgrade friction between the last anchor and the point of fixity can be assumed concentrated at several separate points.

Numerical Example. —The following calculations are for a system of 1-in. width. The following dimensional quantities are chosen:

End movement, $\delta_0 = 0.4$ in.

Anchor depth, H = 60 in.
Anchor thickness, t_a = 16 in. (rectangular anchor)

The following soil properties are assumed:

Horizontal coefficient, K_a = 200 psi
Vertical coefficient, K_s = 100 psi
Internal friction angle, ϕ = 32^0
Cohesion, c = 10 psi
Effective unit weight, $\bar{\gamma}$ = 120 pcf = 0.0695 pci

The following concrete properties are assumed:

Elastic modulus, E = 4×10^6 psi
Poisson's ratio, ν = 0.15
Thermal coefficient, α = 7×10^{-6} per deg. F
Unit weight, γ_c = 150 pcf = 0.0868 pci

A strain due to a pavement temperature increase of 50^0 F is assumed. Moisture and chemical strain are assumed zero. Thus the strain to be restrained is $\epsilon = 50 \times 7 \times 10^{-6} = 3.5 \times 10^{-4}$. The subgrade friction curve shown in Figure 19 is assumed.

Anchor spacing is calculated as follows:

$$\frac{2C}{\bar{\gamma}} \tan\left(45^0 + \frac{\phi}{2}\right) = \frac{2 \times 10}{0.0695} \tan\left(45^0 + \frac{32^0}{2}\right) = 512 > 60 \text{ in.}$$

Therefore, use Eq. 16.

$$L' = \frac{\frac{\bar{\gamma} H}{2c} \tan^2\left(45^0 + \frac{\phi}{2}\right) + 2 \tan\left(45^0 + \frac{\phi}{2}\right)}{\frac{\bar{\gamma} \tan}{c} + \frac{1}{H}} = \frac{\frac{0.0695 \times 60}{2 \times 10}(1.804)^2 + 2(1.804)}{\frac{0.0695}{10}(0.625) + \frac{1}{60}} = 204 \text{ in.}$$

Adding the anchor thickness of 16 in. gives a spacing L of 220 in. center to center.

Limiting anchor resistance by Eq. 40 is

$$P_s' = L'(c + \bar{\gamma} H \tan\phi) = 204(10 + 0.0695 \times 60 \times 0.625) = 2,570 \text{ lb}$$

$$\frac{P_s'}{2} = \frac{2,570}{2} = 1,285 \text{ lb} = \text{maximum shear}$$

Maximum anchor moment by Eq. 47 is

$$M_o = \frac{2}{3} PH = \frac{2}{3} \times 1,285 \times 60 = 51,400 \text{ in.-lb}$$

The 16-in. anchor thickness is sufficient.

Maximum slab moment and shear due only to M_o (that is, neglecting axial and traffic loads on slab) are assumed to be twice those values given by Eqs. 50 and 51.

$$\text{Max. } M = \frac{2 M_o}{2} = 51,400 \text{ in.-lb}$$

$$\text{Max. } V = \frac{2 M_o}{2} \beta_s = 51,400 \times 0.0164 = 843 \text{ lb}$$

The value β_s = 0.0164 per in. is taken from Figure 10, assuming a 10-in. thick slab adjacent to the anchors. A 10-in.

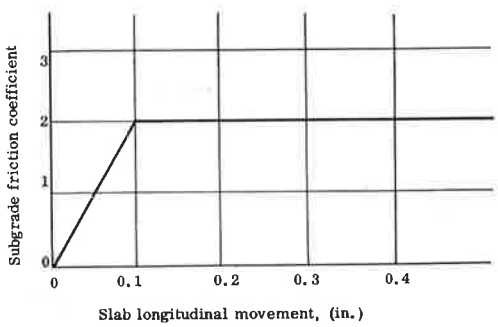

Figure 19. Assumed subgrade friction curve for numerical example.

slab can resist the moment if double reinforcing is provided near the anchor. The slab would have a theoretical shear stress due to the anchor moment, of about 103 psi, which is assumed satisfactory for this example.

Joint moment-rotation ratio C from Figure 7 is 2.27×10^7 in.-lb. The ratio

$$\frac{K_a}{C} = \frac{200 \text{ lb/in.}^2}{2.27 \times 10^7 \text{ in.-lb}} = 0.0000088/\text{in.}^3$$

From Figure 10, $\beta_a = 0.0138$ per in.

Elastic anchor resistance constant R is interpolated from Figure 9 as shown in Figure 20. For each of the four values of K_a/C plotted in Figure 9, one point is plotted in Figure 20. The values are read from Figure 9 for an H of 60 in. and are interpolated by eye for a β_a of 0.0138 per in. Thus Figure 20 is a plot of R vs K/C for an H of 60 in. and a β_a of 0.0138. The value of R for the present example is read from Figure 20 to be 0.683.

$$R = \frac{P}{H K_a \delta} = 0.683$$

thus,

$$P = 0.683 \times 60 \times 200\,\delta = 8,200\,\delta \text{ lb per in.}$$

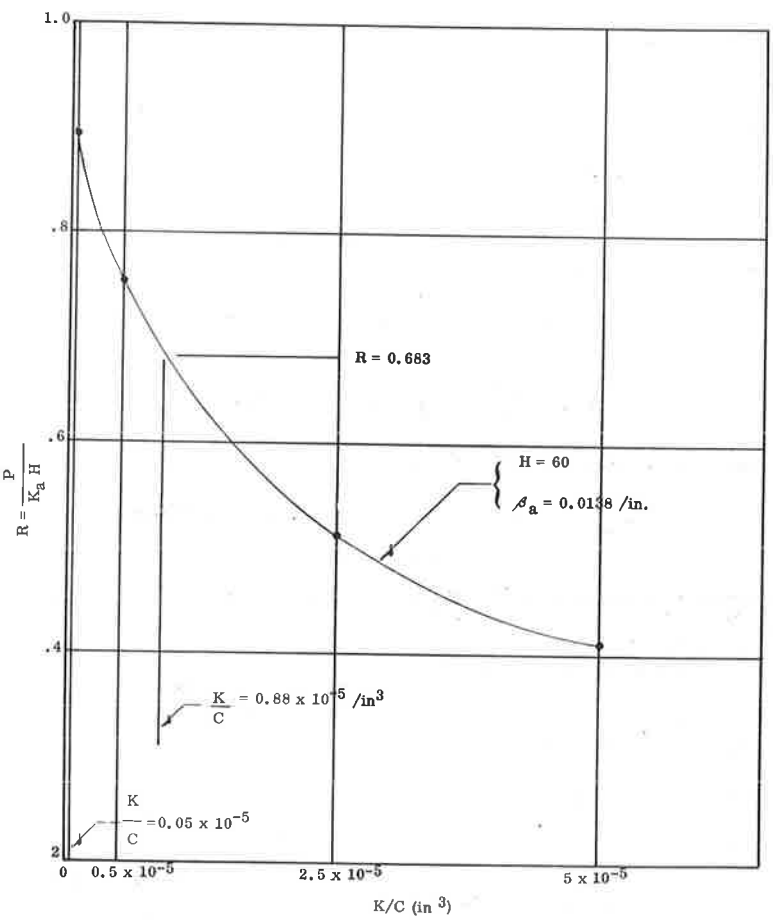

Figure 20. Longitudinal movement of slab in numerical example.

Longitudinal movement:

$$\delta_o = 0.4 \text{ in.}$$

At first anchor located H = 60 in. from the end

$$\delta_1 = \delta_o - \epsilon H = 0.400 - 0.00035 \times 60 = 0.379 \text{ in.}$$

$$P = 8,200 \times 0.379 = 3,110 \text{ lb} > \frac{P_s'}{2} = 2,570 \text{ lb}$$

therefore,

$$P_1 = 2,570 \text{ lb}$$

At second anchor located 220 in. from first anchor

$$\delta_2 = \delta_1 - \epsilon L + \left(\frac{P_1 L}{AE}\right)$$

$$= 0.379 - 0.00035 \times 220 + 2,570 \left(\frac{220}{10 \times 4 \times 10^6}\right)$$

$$= 0.379 - 0.077 + 0.014 = 0.316 \text{ in.}$$

and

$$P = 8,200 \times 0.316 = 2,590 > \frac{P_s'}{2} = 2,570 \text{ lb}$$

therefore,

$$P_2 = 2,570 \text{ lb}$$

$$\delta_3 = \delta_2 - \epsilon L + (P_1 + P_2) \frac{L}{AE}$$

$$= 0.316 - 0.077 + (2,570 + 2,570) \left(\frac{220}{10 \times 4 \times 10^6}\right)$$

$$= 0.316 - 0.077 + (5,140)\,(55 \times 10^{-7}) = 0.267 \text{ in.}$$

$$P = 8,200 \times 0.267 = 2.190 \text{ lb} < \frac{P_s'}{2} = 2,570 \text{ lb}$$

therefore,

$$P_3 = 2,190 \text{ lb}$$

$$\delta_4 = \delta_3 - \epsilon L\,(P_1 + P_2 + P_3)\ \frac{L}{AE}$$

$$= 0.267 - 0.077 + (7,330)\,(55 \times 10^{-7}) = 0.230 \text{ in.}$$

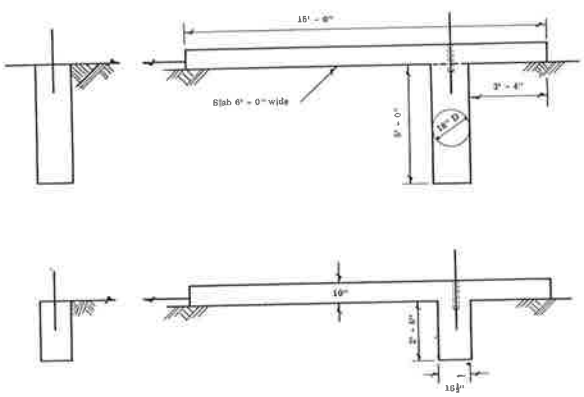

Figure 21. Four anchor units tested.

$$P_5 = 8,200 \times 0.204 = 1,670 \text{ lb}$$

$$\delta_6 = \delta_5 - \epsilon L + (P_1 + P_2 + P_3 + P_4 + P_5) \frac{L}{AE}$$

$$= 0.204 - 0.077 + (10,880)(55 \times 10^{-7}) = 0.187 \text{ in.}$$

The longitudinal movments of points 1 through 6 are shown in Figure 18. By Eq. 56 the required total restraining force, assuming a slab thickness of 10 in. throughout the pavement length, is

$$\Sigma P = A E \epsilon = 10 \times 4 \times 10^6 \times 3.5 \times 10^{-4} = 14,000 \text{ lb}$$

If a thinner pavement had been assumed outside the region of the anchors, the corresponding area would have been used to calculate the required ΣP.

Anchors 1 through 5 develop a resistance of 10,880 lb. The line from point 6 to 8 is a straight extension of the line from point 5 to point 6. The theoretical movement curve would actually fall above line 6-8. But by assuming that the movement is as indicated by line 6-8, and by assuming that the subgrade friction coefficient is as shown in Figure 19 the subgrade resistance between points 6 and 8 can be determined. Between points 6 and 7 subgrade resistance is

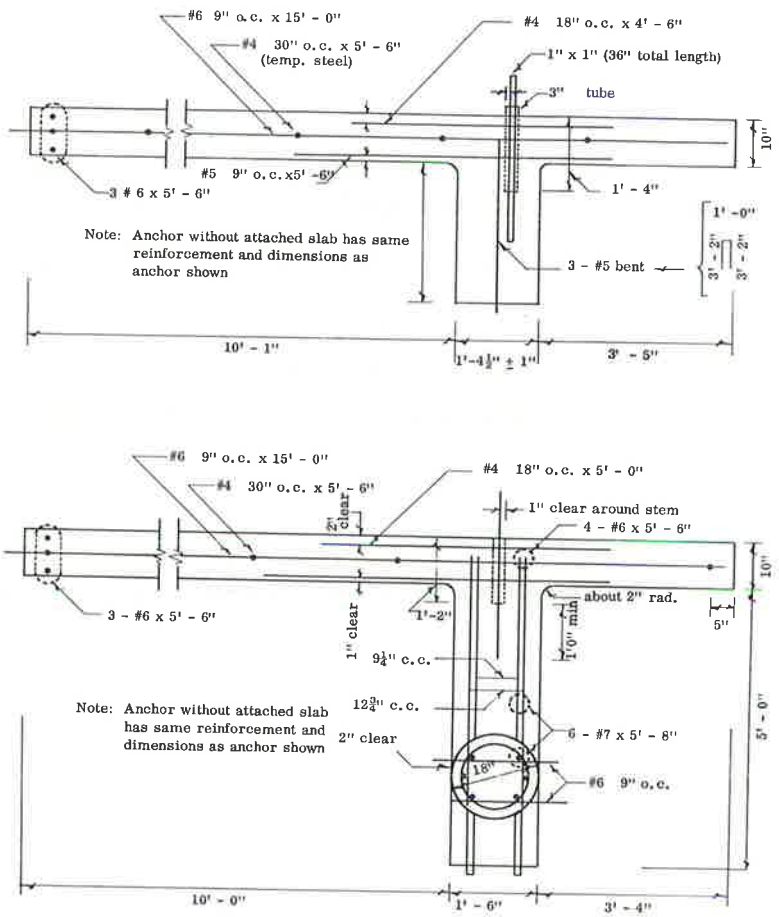

Figure 22. Structural details of test anchors.

$$P_{6-7} = 2 \times 0.0868 \times 10 \times 1,126 = 1,950 \text{ lb}$$

Between points 7 and 8 the subgrade resistance is

$$P_{7-8} = 1 \times 0.0868 \times 10 \times 1,294 = 1,120 \text{ lb}$$

Thus, the total restraining force at point 8 is

$$10,880 + 1,950 + 1,120 = 13,950 \text{ lb}$$

Because subgrade friction would actually deflect curve 6-8 upward and thus induce even greater subgrade friction, it is safe to assume the design using five anchor units is sufficient. A more precise incremental analysis between point 6 and some point of fixity beyond point 8 might even indicate that four anchor units would be sufficient. If the pavement thickness beyond the anchor region had been 8 in. rather than 10 in., a system of four anchor units would very likely have been sufficient.

FIELD EXPERIMENT

The four units shown in Figure 21 were built and tested during the summer and fall of 1961. Trenches and cylindrical holes dug with hand tools served as forms for the concrete. The two slabs were cast monolithically with their anchors. Structural details of the units are shown in Figure 22.

Known horizontal forces were applied as shown in Figure 21. Horizontal and vertical anchor movement, anchor rotation, and slab vertical deflection were measured.

Soil Properties

Subgrade soil at the test site was a brownish red clay having a fairly uniform appearance. Nine samples indicated liquid limits from 37 to 48 with a mean of 42, plasticity indexes from 16 to 25 with a mean of 21, and water contents from 17 to 33 with a mean of 28 (all in percent). One gradation analysis indicated 80 percent passing the No. 200 sieve.

The results of triaxial tests on samples taken from each anchor site are given in Table 1. Samples were taken with a 2-in. diameter split-spoon sampler. There is some uncertainty about the results for c and ϕ because they are based on tests run on but three or four different samples from each anchor site, each tested at a different chamber pressure.

A plate-bearing test was made at the site of each of the slabs. For these tests, an 18-in. diameter plate was loaded in 2,000-lb increments until a settlement of over 0.8 in. developed. The load-settlement curves are shown in Figure 23. The subgrade modulus K_0 corresponding to the straight line 0_a in Figure 23 is about 74 pci.

Loading System

The applied force was developed by a screw jack (Fig. 24) extending to develop a tensile load in a steel frame tied to two adjacent anchors. In Figure 25 load is being applied to the rectangular anchor in the foreground and to the rectangular anchor and

TABLE 1

TRIAXIAL TEST RESULTS

Anchor Site	No. of Samples	Cohesion, c (psi)	Angle of Friction, ϕ (°)	Unconfined Compressive Strength (psi)
Rectangular:				
With slab	4	9	44	41
Without slab	3	9	16	23
Cylindrical:				
Without slab	4	5	36	24
With slab	3	11	37	45

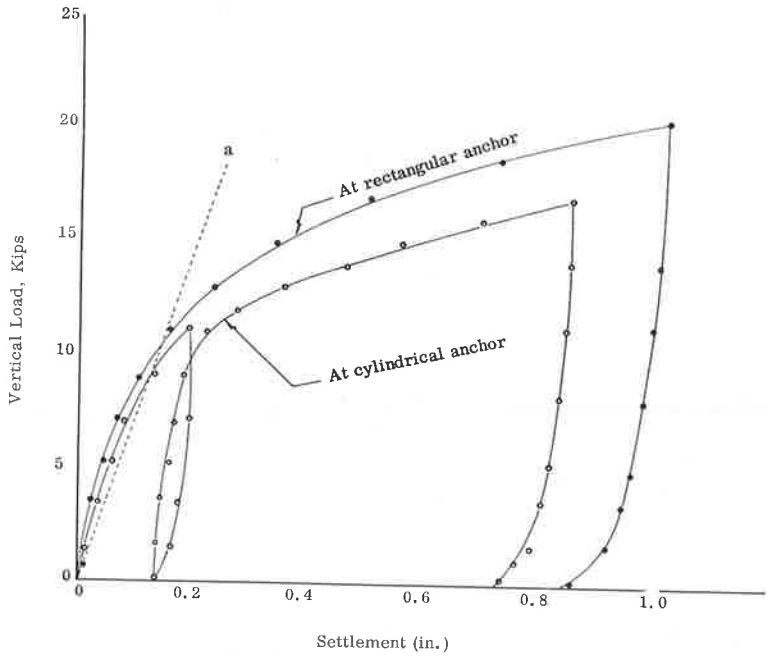

Figure 23. Load settlement curve for 18-in. circular plate bearing test.

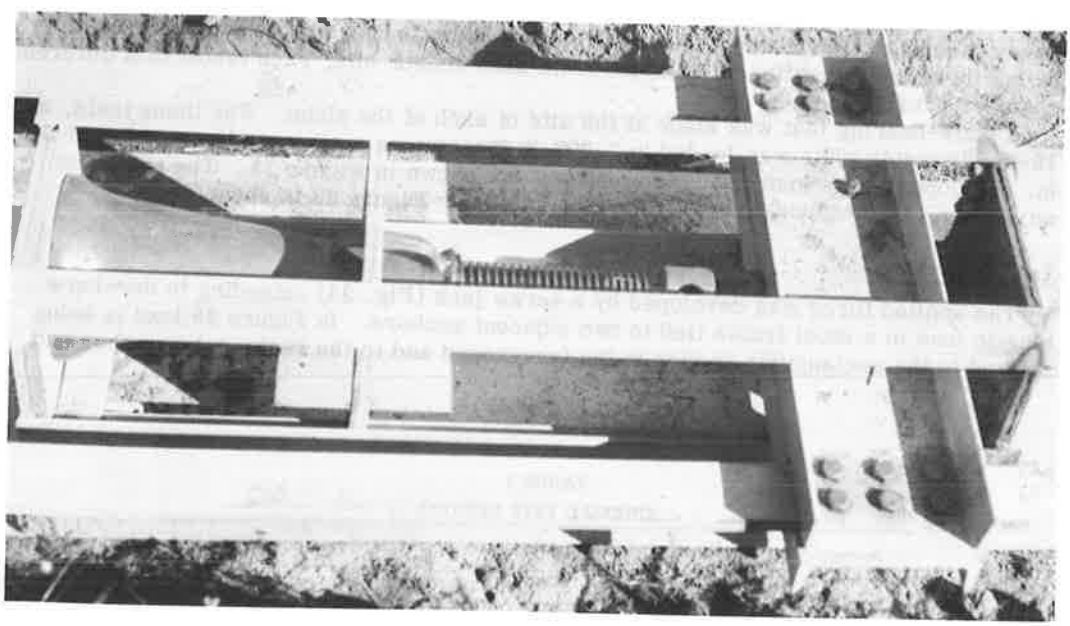

Figure 24. Screw jack for loading system.

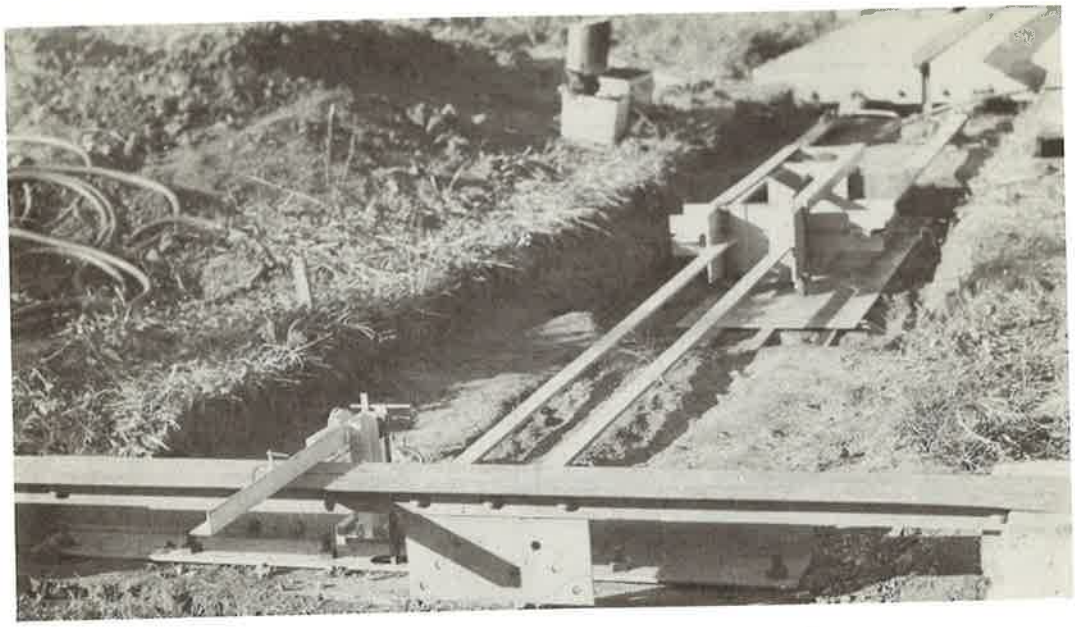

Figure 25. Load being applied to rectangular anchors.

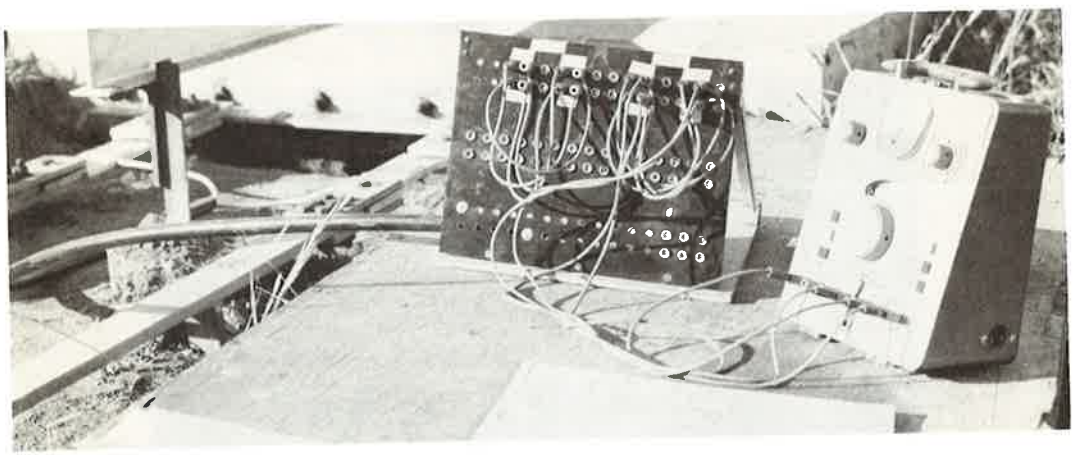

Figure 26. Load cells, wiring, and strain indicator.

slab in the background (the open crack in the soil behind the anchor is noteworthy). The tensile load in the steel frame was measured by two precalibrated load cells. The load cells were pin-connected flat bars with electrical resistance wire strain gages attached. The cells can be seen attached to the slab and long steel tensile members to the left in Figure 26.

Loads were generally applied in increments of 2,000 to 4,000 lb. The total time required for a load cycle ranged from 50 to 140 min. Peak loads were never held for more than a few minutes at the most.

Deflection and Rotation Measurements

Dial micrometers were used as shown in Figure 27 to measure deflection and rotation of the anchor units. A foot was attached at right angles to the stem of each

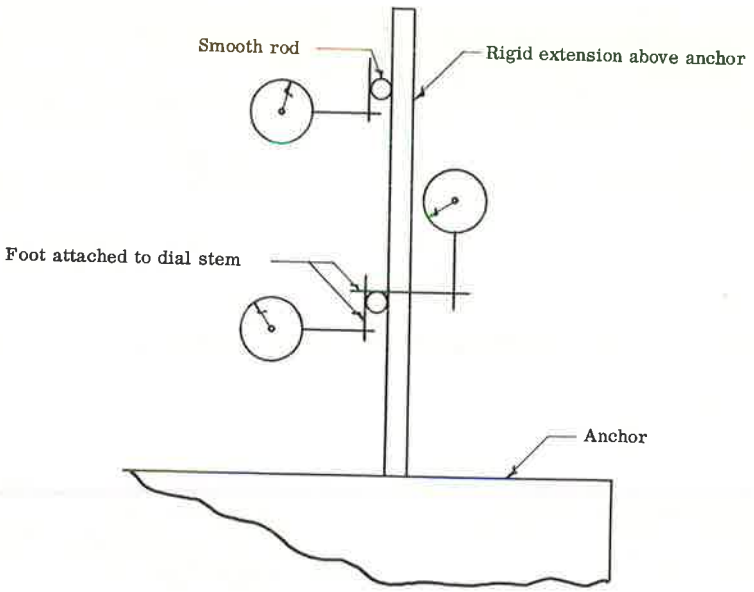

Figure 27. Schematic arrangement of dial micrometers above anchor.

Figure 28. Micrometers in position for measuring horizontal translation and rotation.

micrometer used. This foot remained in contact with a smooth horizontal cylindrical rod attached to a rigid extension to the anchor. Thus, only the horizontal or vertical component of translation of the cylindrical rod was indicated on the dial. By measuring the horizontal movement of two points, and the vertical movement of one of the points, the translation and rotation of the top of the anchor were determined. Two micrometers for measuring horizontal translation and rotation are shown in Figure 28. The vertical micrometer is hidden behind the rigid extension to the anchor.

The micrometers used to measure vertical slab deflection are shown in Figure 29. They also had feet attached at right angles to the stem. The dials indicated only the vertical component of translation of cylindrical rods attached to the slab.

Experimental Results

Figure 30 shows plots of the horizontal deflection of the top of the various test units vs the applied horizontal force. The figure shows the results for all load cycles of the units without slabs but only for one cycle each for the units with slabs.

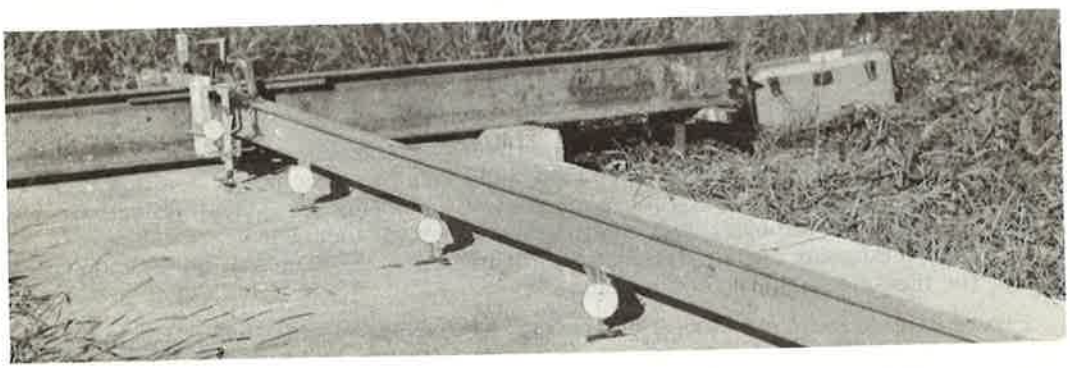

Figure 29. Micrometers in place for measuring vertical slab deflection.

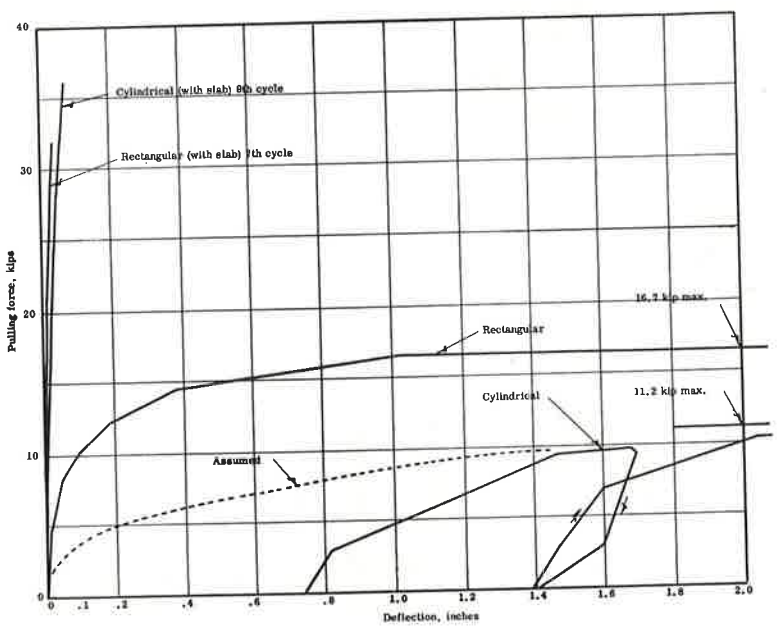

Figure 30. Load vs horizontal deflection at top of anchors.

The dashed curve in Figure 30 represents the assumed initial cycle of the cylindrical unit without slab. For that cycle, a usable load record was not obtained because of an unknown electrical resistance in the strain gage circuit. The deflections for that cycle were measured and the loads and deflections for the two subsequent cycles were determined as plotted.

The figure also suggests that there is a great difference in strength of an anchor with slab as compared to an anchor without attached slab, but the curves might be misleading without further explanation. The total horizontal force applied at the slab end is the quantity plotted in the figure. This total force no doubt included a slab subgrade friction component which unfortunately was not evaluated. Subgrade friction could conceivably account for perhaps 50 percent of the force applied to the slabs.

The resistance of the slab to rotation of the slab-anchor joint accounts for a large part of the strength of a slab-anchor combination. An infinitely stiff anchor in an elastic subgrade, if permitted no joint rotation, would be four times as strong as a similar anchor with free joint rotation. Less stiff anchors under similar conditions have a comparable strength ratio of less than four with the strength ratio decreasing as stiffness decreases. Eq. 31 is a statement of this phenomenon.

Other factors contributing to the great strength of the anchors tested with attached slabs might be (a) the confinement by the slab of the soil in front of the anchor, and (b) the decreased vertical movement of the anchor due to slab weight and stiffness.

Figure 31 shows load-deflection curves for all recorded load cycles on the two anchor units with attached slabs. The following characteristics of these curves stand out:

1. The general slopes appear to remain almost constant for subsequent load cycles.
2. On removal of load, the anchors returned almost to their initial position. Backlash in the dial micrometers could explain part of the apparent residual deflection.
3. The curves could be roughly approximated by a straight line.
4. The rectangular anchor developed about twice the resistance of the cylindrical anchor for the same amount of movement.

Figure 31 also suggests a great detraction of the experimental study. Cycle four of the cylindrical anchor and cycle two of the rectangular anchor suggest the initiation of

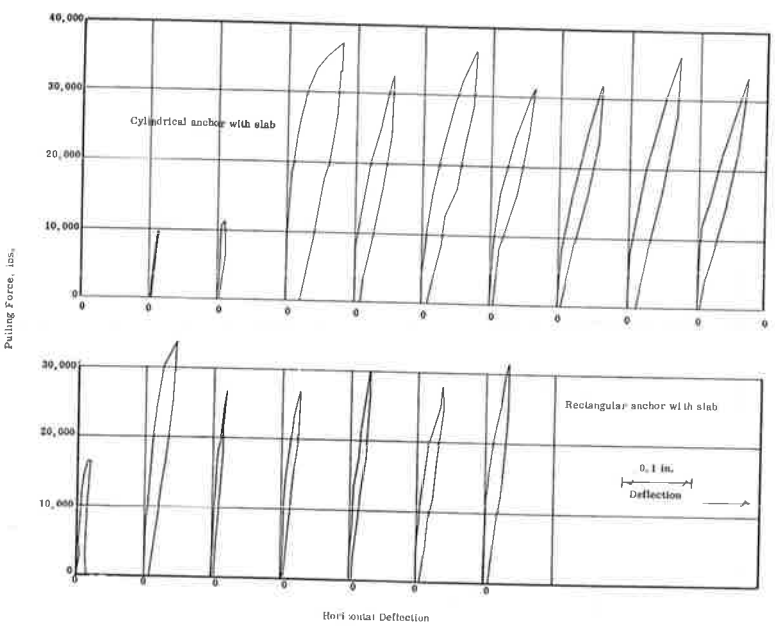

Figure 31. Load vs horizontal deflection at top of anchor with slabs.

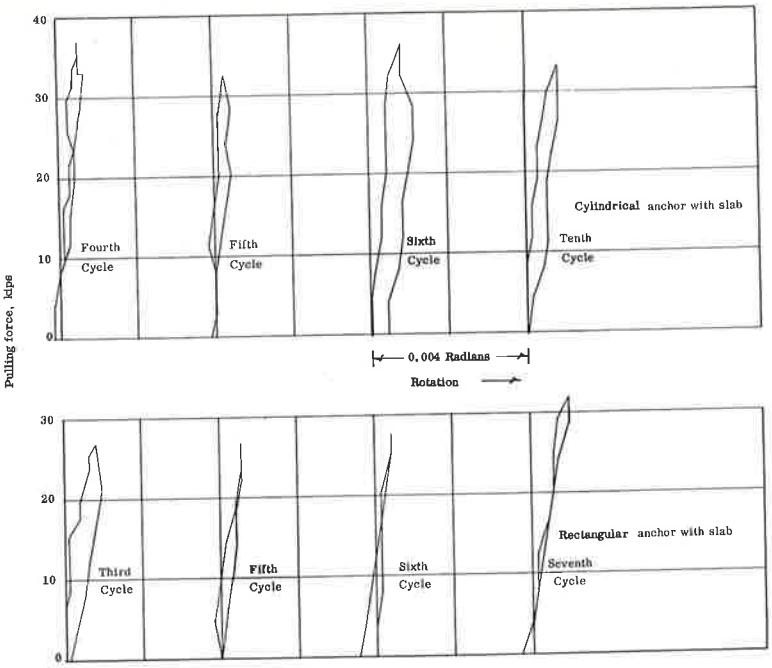

Figure 32. Some of the more characteristic load-rotation curves for anchors with slabs.

some form of plastic yielding. But due to limitations of the loading system, applied horizontal loads did not exceed about 37,000 lb. In this connection it is of interest to compare the peak load of 472 lb per in. applied to the rectangular anchor and slab with that anchor's theoretical limiting load as predicted by Eq. 44. Assuming a cohesion of 9 psi and an internal friction angle of 44^{0} as determined by soil tests (Table 1), and assuming an effective soil unit weight of 120 pcf, an L'/H ratio of about 4.5 is obtained from Figure 13. Substituting into Eq. 44 gives

$$P_S' = L' (c + \overline{\gamma} H \tan \phi) = 4.5 \times 30 (9 + 0.0695 \times 30 \times 0.965) = 1,490 \text{ lb/in. width.}$$

Thus, the maximum load applied during the test was a little less than one-third the limiting plastic resistance predicted by Eq. 44, or a little less than two-thirds the limiting values $P_S'/2$ recommended for design use.

Figure 32 shows some of the more characteristic curves of load vs joint rotation for the anchor units with attached slabs. The rotation values were obtained by dividing the difference in two horizontal dial micrometer readings by the vertical distance between micrometers (Fig. 27). The two dial readings corresponding to the maximum rotation shown in Figure 32 (6th cycle, cylindrical) were 75 and 83. The fact that rotations were determined from two readings that were fairly close together, and that either reading might be in error in either direction, would seem to explain the erratic nature of the curves.

Figure 33 shows the location of the dials

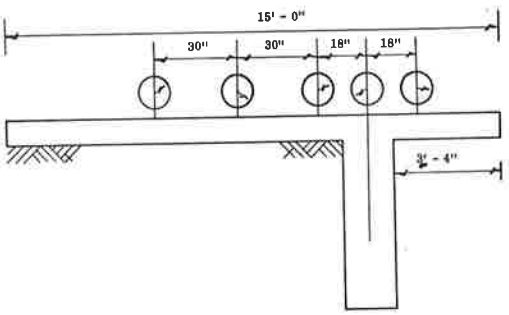

Figure 33. Vertical dial micrometer locations.

used to measure vertical slab deflection. Some representative deflected shapes are shown in Figure 34. The rotation of the top of the anchor is indicated by the downwardly extending element (the upward deflection of the anchor at the joint is noteworthy, as well as the fact that the slab just behind the anchor remained almost at right angles with the anchor, whereas there was significant bending of the slab in front of the anchor).

The curves in Figure 31 show that the rectangular anchor developed about twice the resistance of the cylindrical anchor for the same amount of slab movement. The total volume of the rectangular anchor was about 2.4 times that of the cylindrical anchor, but the cylindrical anchor contained about three times as much steel as the rectangular one. The projected area of the rectangular anchor available to induce subgrade resistance was two times the corresponding projected area of the cylindrical anchor. Thus, a comparison of resistance developed with material quantity for this particular experiment does not indicate one anchor configuration to be particularly superior to the other.

An earlier discussion of longitudinal movement indicated the advantage of developing anchor resistance as near the slab end as possible. Thus, the rectangular anchor might appear to be the better of the two tested in this experiment.

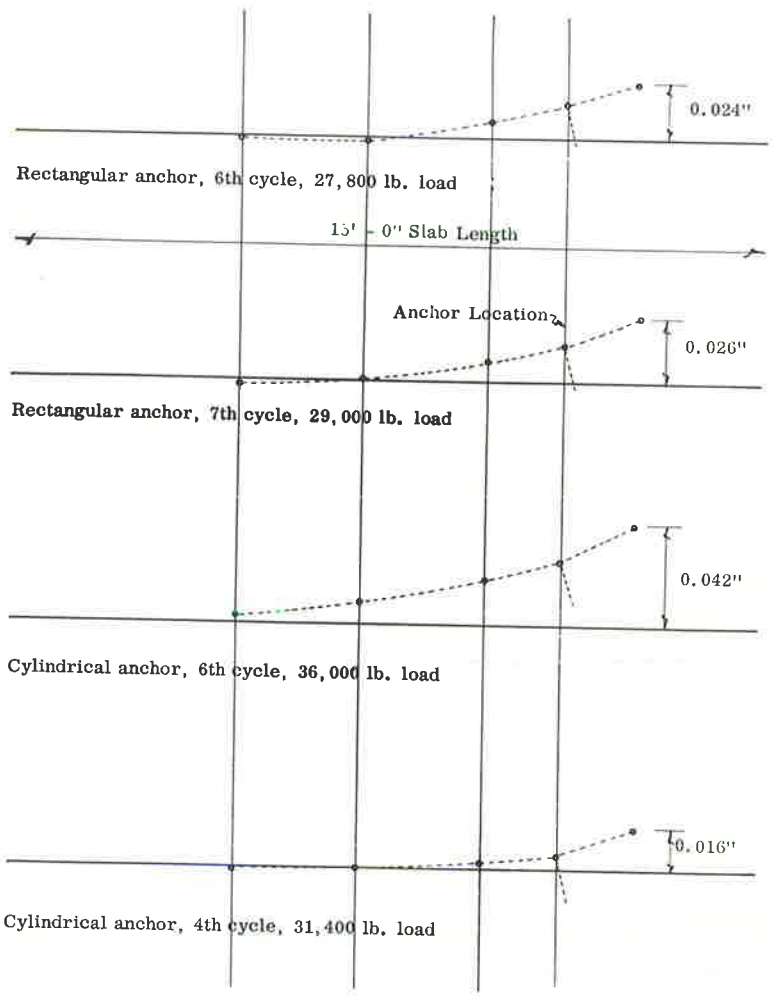

Figure 34. Representative deflected shapes of slabs.

But a general conclusion as to the better configuration, cylindrical or rectangular, cannot be made on the basis of this experiment alone. For example, the results do not indicate whether two or three cylinders of the same dimensions as the one used would be less resistant than a rectangular anchor 60 in. deep.

Significance of Results

Two items of the results are of particular significance relative to the analysis and design of an anchor system. First, the great difference in strength of the anchor units tested (Fig. 30) demonstrates the advantage of providing a rigid joint between anchor and slab. Second, the approximate linearity of the load-deflection curves (Fig. 31) would seem to justify an elastic analysis for the lower load range of anchor response.

APPLICATION TO JOINTED PAVEMENT

When the slabs of a jointed concrete pavement contract, loose soil or other foreign matter may be deposited in the open joints. When the slabs later expand, the deposited solid material may partially prevent the normal closing of the joint. Each cycle of contraction and expansion may result in a greater separation between slabs and a net increase in pavement length. This phenomenon is in contrast to that occurring in a continuously-reinforced concrete pavement whose random cracks are so narrow that very little intrusion of foreign matter takes place.

Shelby and Ledbetter (4) have reported early indications of satisfactory results using only two rectangular anchor units to restrain the ends of jointed pavements. They reason that by preventing the progressive opening of contraction cracks, from the beginning of pavement life, the growth forces are kept much lower than they would be if anchors were not provided.

Some parts of the theoretical analysis previously developed for continuously-reinforced pavement can be applied directly to jointed pavement. The conclusion that subgrade anchor units are most efficient if bunched near the pavement end would apply equally to jointed pavement. The plastic analysis for optimum anchor spacing, Eqs. 45 and 46, would be applicable. The shear and moment analysis might be of some assistance in design.

Application of the elastic anchor resistance analysis would require that longitudinal slab movement at the anchor be calculated or assumed. To adapt the longitudinal slab movement analysis to the jointed pavement problem, it would be necessary to assume the change in width of each joint as well as the pavement end movement. Short of that, it is recommended that jointed pavements be provided with, at most, only a very few anchor units at each end, and that subsequent design be adjusted as indicated by careful observation of field performance.

It is recommended that the anchor units be spaced as indicated by the plastic analysis (Eqs. 45 and 46) and that the entire group be connected by one continuous slab.

CONCLUDING REMARKS

The analysis methods just presented are believed to be suitable for design use in their present form, but they have thus far been correlated with field observations to but a very limited degree. More extensive field observations may indicate a need for modification of the analysis.

Some very useful field observations have been reported in the literature (for example, 4, 9) but further field data are needed, particularly on the performance of subgrade anchor units. It would be desirable to correlate such data with a theoretical analysis such as developed in this paper. For such a correlation, it would be necessary to determine soil and concrete properties, dimensions, temperatures, and absolute longitudinal movements at the slab end, at each anchor unit, and at other points on the pavement slab. It would be desirable to measure any significant vertical slab deflection and carefully to examine for slab cracks in the vicinity of anchor units. For such a study, more meaningful information would probably be obtained from an anchor system that permitted appreciable end movement.

ACKNOWLEDGMENTS

The following major contributions to the project are gratefully acknowledged. W. Zuk made the initial suggestion to the author that the project be undertaken. J. F. Jackson and K. E. McElroy assisted in the planning and execution of the experimental work. K. Tatlidil and G. R. Smith assisted with the many mathematical computations. The manuscript was checked by Y. N. Liu. T. E. Shelburne provided over-all support and encouragement throughout the project.

REFERENCES

1. ASCE, Proc., Research Conference on Shear Strength of Cohesive Soils (June 1960).
2. CRSI, "Design of Continuously-Reinforced Concrete Pavement for Highways." Continuously-Reinforced Concrete Pavement Bull. 1 (Dec. 1960).
3. Hetenyi, M., "Beams on Elastic Foundations." University of Michigan Press (1946).
4. Shelby, M. D., and Ledbetter, W. B., "Experience in Texas with Terminal Anchorage of Concrete Pavement." HRB Bull. 332, 26-38 (1962).
5. Teller, L. W., and Sutherland, E. C., "The Structural Design of Concrete Pavement." Public Roads (Oct. 1935).
6. Terzaghi, K., "Theoretical Soil Mechanics." Wiley (1943).
7. Terzaghi, K., "Evaluation of Coefficients of Subgrade Reaction." Geotechnique (Dec. 1955).
8. Terzaghi, K., and Peck, R. B., "Soil Mechanics in Engineering Practice." Wiley (1948).
9. Van Breemen, W., "Ten-Year Report on Experimental Continuously-Reinforced Concrete Pavements in New Jersey." HRB Bull. 214, 41-75 (1959).
10. Zuk, W., "Analysis of Special Problems in Continuously-Reinforced Concrete Pavements." HRB Bull. 214, 1-20 (1959).